ROYAL SOCIETY
OF CHEMISTRY

COMMUNICATION

CrossMark
click for updates

An isoindigo containing donor–acceptor polymer: synthesis and photovoltaic properties of all-solution-processed ITO- and vacuum-free large area roll-coated single junction and tandem solar cells†

Rasmus Guldbaek Brandt,‡[ab] Wei Yue,‡[ab] Thomas Rieks Andersen,[c] Thue Trofod Larsen-Olsen,[c] Mogens Hinge,[d] Eva Bundgaard,[c] Frederik C. Krebs[c] and Donghong Yu*[a]

In this work, the design, synthesis, and characterization of a donor–acceptor polymer from dithieno[3,2-b:2′,3′-d]pyrrole and isoindigo (i-ID) are presented. The synthesized polymer has been applied in the fabrication of large area ITO-free organic photovoltaic devices, both by spin coating and roll coating; the latter was used to construct both single junction and multi-junction organic photovoltaic (OPV) architectures.

In recent years, there has been an increasing focus on the development of electron deficient heteroaromatic moieties for the synthesis of donor–acceptor (D–A) type conjugated polymers for organic photovoltaic devices (OPVs), such as phthalimide (PI),[1] naphthalene diimide (NDI),[2] perylenediimide (PDI),[3] benzothiadiazole (BT) and benzobis(thiadiazole) (BBT),[4] diketopyrrolopyrrole (DPP),[5] benzodipyrrolidone (BDP),[6] thieno[3,4-c]pyrrole-4,6-dione (TPD),[7] and isoindigo (i-ID).[8] When incorporated with donor units (alternating) in the polymer backbone, the electron richness and electron deficiency ensure a low band gap, thus allowing for more efficient absorbance of incident solar photons over a wider part of the solar spectrum.[9]

Electron deficient monomers are essential for the design of low band gap (LBG) conjugated polymers, as such moieties in the polymer main chain exhibit high electron affinity and strong ability to reduce the band gaps of D–A polymers compared to the corresponding homo-polymers. They can especially tune the energy level of the lowest unoccupied molecular orbital (LUMO) of the given polymer, which is the key parameter, being associated with the charge transfer process in OPVs. The optimal driving force for the charge transfer process has been commonly recognized as 0.3 eV, *i.e.* the LUMO energy difference between the donor (such as in D–A polymers) and the acceptor (state-of-the-art phenyl-C_{61}-butyric acid methyl ester (PC[60]-BM)).[10] Among those previously mentioned acceptor moieties, i-ID is especially interesting as an efficient acceptor block; due to its strong electron-withdrawing characteristics and a large optical transition dipole, the interest was first sparked by Reynolds *et al.*[11] who showed that an i-ID containing oligothiophene can be used as a p-type OPV material, with a power conversion efficiency (PCE) of 1.76%. Independent reports have been published since 2011 by Zhang *et al.*,[12] Liu *et al.*,[13] and Wang *et al.*[14] with PCE ranging from 1 to 3%, the high PCE of 6.3% was obtained by Wang *et al.*[15] in 2011. This was until very recently the best performing i-ID containing polymer, but it was overtaken by Geng *et al.*[16] who reported a PCE of 8.2% in 2014, which is now the highest PCE for i-ID based LBG polymers. On the other hand, for D–A LBG conjugated polymers, the fused ring donor unit dithieno[3,2-b:2′,3′-d]pyrrole (DTP) is a widely used electron rich moiety and has been proven to have excellent electron donating properties and good molecular planarity. A similar D–A combination of bisthiophene–DTP (BT–DTP) has been reported by Wu *et al.*, poly(bisthiophenedithieno[3,2-b:2′,3′-d]pyrrole-isoindigo) (**PBTDTPI**) afforded OPV devices with efficiencies in the range of around 1.86%.[17] However, all the above-mentioned "hero" i-ID based LBG polymer solar cells including **PBTDTPI** are single junction solar cells with small active areas (not exceeding 0.1 cm²) on rigid glass substrates using ITO as the semitransparent front electrode and vacuum evaporated metal back electrode. Indium scarcity, its high market demand and the high energy input required for ITO production using vacuum techniques have become the bottlenecks in developing/commercializing OPV devices due to the resulting non-sustainability, high cost and high energy payback time.[18] Therefore the replacement of indium becomes essential

[a] *Department of Chemistry and Bioscience, Aalborg University, Fredrik Bajers Vej 7H, DK-9220, Aalborg East, Denmark. E-mail: yu@bio.aau.dk*

[b] *Sino-Danish Centre for Education and Research (SDC), Niels Jenses Vej 2, DK-8000, Aarhus, Denmark*

[c] *Department of Energy Conversion and Storage, Technical University of Denmark, Frederiksborgvej 399, DK-4000, Roskilde, Denmark*

[d] *Department of Engineering, Aarhus University, Hangoevej 2, 8200 Aarhus N, Denmark*

† Electronic supplementary information (ESI) available. See DOI: 10.1039/c4tc02877e

‡ These authors contributed equally to this work.

This journal is © The Royal Society of Chemistry 2015

J. Mater. Chem. C, 2015, **3**, 1633–1639 | **1633**

and the substitute should preferably be a solution-based ambient processable system. A possible combination of poly(3,4-ethylenedioxythiophene):polystyrene sulfonate (PEDOT:PSS) with a metal grid remaining on flexible plastic (*e.g.* PET) substrates turns out to be the most readily scalable, facile alternative to ITO coated glass.[18] Large area ITO- and vacuum-free OPV device can be fabricated in a fast and scalable manner by roll-to-roll (R2R) slot-die coating, which has been identified and explored using a large array of techniques by few groups, but with great success so far. However, all but a few reports have used poly(3-hexylthiophene) (**P3HT**) as a polymer donor.[19] Although the above-introduced i-ID containing D–A LBG polymers have outperformed **P3HT** with regard to PV performance with PCEs up to 7.2%, there is no guarantee on transferring this high PV performance when upscaled to a R2R setting from conventional spin-coating and vacuum deposition techniques. It is due to the inherent differences in processing, many of the achievements for small area OPV devices are likely to prove difficult to reproduce using the R2R methods. In order to minimize/close this gap of knowledge, more effort must be devoted to the testing of new promising materials in R2R fabricated PSCs. As a consequence of the discrete nature of the absorbance bands of conjugated organic molecules, a necessity to absorb different regions of the solar spectrum emerges. To capture the entirety of the solar spectrum, tandem solar cells with compensated light absorption can be employed. Such a tandem structure will in principle lead to a higher performance than the single junction in spite of the expense of extra processing steps and enhanced material consumption. In this paper, a novel D–A polymer **PDTPI** incorporating DTP and i-ID as donor and acceptor moieties, respectively, was successfully synthesized *via* Pd-catalyzed Stille coupling reaction. Vacuum- and ITO-free OPV devices from **PDTPI** have been roll-coated as single junction and tandem solar cells with **P3HT** and **PBDTTTz-4** in the area scale of 1 cm², and the photophysical and electrochemical properties of **PDTPI** and photovoltaic properties of spin coated single junction and roll coated large area (∼1 cm²) single junction and tandem cells were fully investigated.

Experimental

Materials and synthesis

The monomers 2,6-di(trimethyltin)-*N*-(1-pentylhexyl)dithieno [3,2-*b*:2′,3′-*d*]-pyrrole and 6,6′-dibromodi(2-ethylhexyl)isoindigo were synthesized following the procedures reported in the literature.[11,20] Poly-3-hexylthiophene (**P3HT** from Plextronics) had a M_n of 40 000 Da. **PBDTTTz-4** was synthesized according to literature procedures,[37,38] phenyl-C_{61}-butyric acid methyl ester (PC[60]BM, from Solenne) had a purity of 99%. PEDOT:PSS was purchased from Agfa (Orgacon EL-P 5010), or Heraeus (Clevious P VP Al 4083 and Clevious F-010). Electron transport layers (ETL) were coated using a stabilized ZnO nanoparticle solution in acetone. Thermally curable Ag (PV-410) was purchased from Dupont. All other chemicals were used as received, unless noted.

Polymerization of PDTPI

A mixture of 2,6-di(trimethyltin)-*N*-(1-pentylhexyl)dithieno [3,2-*b*:2′,3′-*d*]-pyrrole (104.30 mg, 0.158 mmol), 6,6′-dibromodi(2-ethylhexyl)isoindigo (100.00 mg, 0.155 mmol), tris(dibenzylideneacetone)dipalladium (Pd₂(dba)₃, 2.84 mg, 3.10 μmol), and tri-*o*-tolylphosphine (P(*o*-Tol)₃, 7.55 mg, 24.8 μmol) was preliminarily degassed with N₂, and then toluene (16 mL) was added. The mixture was further purged with N₂ for 20 min and heated to 120 °C for 48 h. Subsequently the reaction was cooled to room temperature and the solution was precipitated in methanol. The crude polymer was collected by filtration and then purified on a Soxhlet extractor using acetone and hexane in succession. The polymer was extracted with chloroform and obtained by precipitating the chloroform solution in methanol, yielding 105 mg (55%) solid dark polymer. GPC: 8860 Da; PDI 1.52. ¹H NMR (600 MHz, CDCl₃, δ, ppm): 9.11 (d, 2H), 6.65–7.31 (m, 6H), 4.39 (s, br, 1H), 3.75 (s, br, 4H), 0.95–2.27 (m, br, 52H).

Measurements

¹H NMR spectra were recorded on a Bruker AvanceIII 600 MHz spectrometer. High temperature gel permeation chromatography (HT-GPC) measurements were conducted on PL-GPC220 equipment at 150 °C with 1,2,4-trichlorobenzene as eluent and polystyrene as standards. Thermogravimetric analysis (TGA) was carried out on a PerkinElmer STA6000 simultaneous thermal analyzer at a heating rate of 10 °C min⁻¹ under nitrogen flow. UV-vis absorption was recorded on a Varian 50 Bio UV-vis spectrophotometer. Cyclic voltammetry (CV) was performed on a CHI660B electrochemical analyzer (CH Instruments) using a three-electrode cell set-up with 0.1 M TATBF₄ in acetonitrile as the electrolyte at a scan rate of 1 V s⁻¹. A glassy carbon working electrode with a diameter of 1 mm, a platinum-counter electrode, and an Ag/Ag⁺ pseudo reference electrode were applied. The potential was calibrated against the ferrocene/ferrocenium redox couple (Fc/Fc⁺, 4.8 eV below the vacuum level). The highest occupied molecular orbital (HOMO) and the lowest unoccupied molecular orbital (LUMO) were estimated by the equations: $HOMO = -(4.80 + E_{ox}^{onset})$ and $LUMO = HOMO + E_{bg}^{optical}$.

Solar cell fabrication and characterization

Spin-coated single junction solar cell

Single junction devices were prepared on a flexible poly(ethylene terephthalate) (PET) substrate using a highly conductive PEDOT:PSS (Heraeus Clevious PH1000) for charge collection, the electron transport layer (ETL) was spin-coated using an aluminium doped ZnO nanoparticle solution in acetone (49 mg mL⁻¹) at 1000 rpm followed by spin coating of a dichlorobenzene solution of **PDTPI** : PC[60]BM (1 : 2, 20 mg mL⁻¹) at 600 rpm. The hole transport layer (HTL) of PEDOT:PSS (Agfa EL-P-5010 : isopropanol 2 : 1 w/w) was spin-coated at 3000 rpm, and finally Ag was vacuum evaporated as the back electrode (Ag). The active area of the OPV cell was 0.25 cm².

1634 | *J. Mater. Chem. C*, 2015, **3**, 1633–1639

This journal is © The Royal Society of Chemistry 2015

Roll-coated single junction solar cells

All roll coated devices were printed on a substrate known as the Flextrode comprising PEDOT:PSS (Heraeus Clevious PH1000) and ZnO on a barrier material with a large scale roll-to-roll flexographic printed silver grid electrode. The active layer **PDTPI** : PC[60]BM (1 : X) and HTL PEDOT:PSS (Clevious P VP Al 4083 and Clevious F-010) were all slot-die coated as reported by Andersen *et al.*[21,22] The back silver electrode was applied by flexographic printing of a heat curing silver paste PV410 (Dupont) as previously reported.[22] All cells possess an active area of 1 cm². All layer thicknesses can be seen in ESI Table S1.†

Roll-coated tandem solar cells

Tandem cells were coated by a method comparable to that used for roll-coated single junction solar cells as described above. LBG polymers **PBDTTTz-4** : PC[60]BM (1 : 1) and **PDTPI** : PC[60]BM (1 : 2) were slot-die coated as the first and second active layers, respectively, isolated by PEDOT:PSS F010, Al 4083 and ZnO layers in between. To minimize the risk of solvent penetration through the intermediate layer the second active layer was coated at 60 °C for faster evaporation. Prior to flexographic printing of the silver electrode, three PEDOT:PSS layers namely F010, 4083 and F010 (seen above) were employed by slot-die coating. Detailed printing processes were described by Andersen *et al.*[21,22] All layer thicknesses can be found in ESI Table S2.†

Solar cell performance

Solar cells were measured with a Keithley 2400 source meter under a KHS 575 solar simulator with an AM1.5G 1000 W m⁻² intensity. The external quantum efficiency (EQE) was determined using a QEX10 system (PV Measurements).

Results and discussion

Synthesis

The structures and synthetic route to the **PDTPI** polymer are illustrated in Scheme 1. **PDTPI** was synthesized *via* Stille cross-coupling reaction between 2,6-di(trimethyltin)-*N*-(1-pentylhexyl)-dithieno[3,2-*b*:2′,3′-*d*]-pyrrole and 6,6′-dibromodi(2-ethylhexyl)-isoindigo that were prepared according to the literature procedure,[11,20] resulting in a reasonable reaction yield of 55%. The obtained polymer had a relatively low M_n of 8860 g mol⁻¹ resulting from the poor solubility of **PDTPI** in toluene. The thermal decomposition temperature (5% mass loss) was found
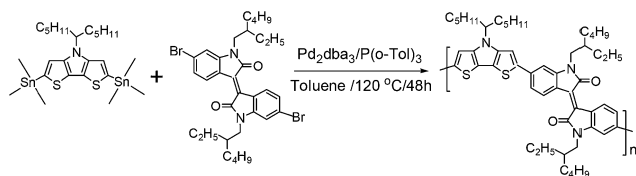
to be 388 °C (see ESI Fig. S1†), providing a sufficient thermal stability for device fabrication and application.

Photophysical properties

Fig. 2 presents the UV-vis absorption spectrum of **PDTPI** acquired in both chloroform solution and thin film. Compared to the weak absorption for the π–π* transition in the high energy band range of 300–500 nm, the intense absorption in the low-energy band range of 550–900 nm evidences a strong electron-withdrawing effect of the i-ID moiety and the intramolecular charge transfer (ICT) between DTP and i-ID entities. As depicted, the maximum absorption bands of **PDTPI** in solution were obtained at 400 and 820 nm, while in film they were unusually blue-shifted to 390 and 790 nm. We suppose that such blue shifts in the absorption of polymer films may originate from two possible aspects: (a) the aggregation of the polymer chains formed in solution; or (b) the presence of two branched alkyl chains on both the D and A moieties, in particular on the i-ID unit, has a larger effect on the spatial arrangement of the copolymers to retard the intermolecular π–π interactions, therefore weak π–π stacking could be assumed. For the former, we have reported, in our previously published work the blue shifts of 5–19 nm from solution to film absorption on D–A LBG polymers comprising dithieno[3,2-*b*:2′,3′-*d*]pyrrole as the donor unit and phthalimide or thieno[3,4-*c*]pyrrole-4,6-dione as the acceptor.[20] This has been further proved by a blue-shift of 5–13 nm in chlorobenzene (CB) solution absorption of the same polymers at 70 °C, compared to
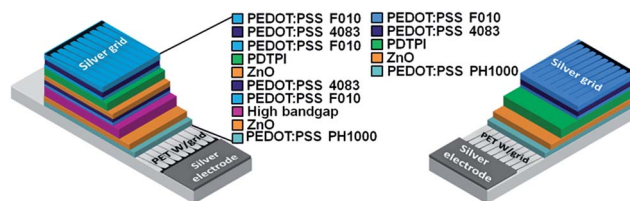
Fig. 1 Schematic structure of the slot-die coated tandem solar cell (left) and the single junction solar cell (right).
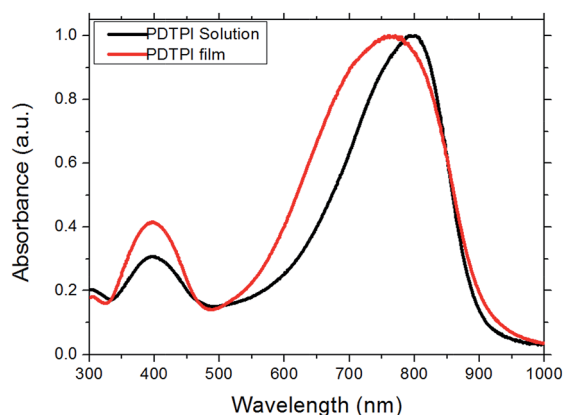
Fig. 2 UV-vis spectra of **PDTPI** in chlorobenzene solution (black line) and film (red line).

Scheme 1 Stille cross-coupling of 2,6-di(trimethyltin)-*N*-(1-pentyl-hexyl)dithieno[3,2-*b*:2′,3′-*d*]-pyrrole and 6,6′-dibromodi(2-ethyl-hexyl)-isoindigo affording the polymer **PDTPI**.

This journal is © The Royal Society of Chemistry 2015

J. Mater. Chem. C, 2015, **3**, 1633–1639 | **1635**

those measured at 25 °C also in CB. Such blue shifts in solution could be attributed to breakup of interchain aggregates in solution at the elevated temperature[23,24] also as suggested by another report on poly-benzodipyrrolidone and dithieno[3,2-*b*:2′,3′-*d*]pyrrole.[6] For the latter, as reported by Su *et al.*, the existence of aliphatic segments on poly(cyclopentadithiophene-*alt*-isoindigo) in the form of both long linear- and short branched-side chains on either donor or acceptor units has proven the same blue-shift of low-energy band absorption from solution to films.[25] Stalder *et al.* observed a similar phenomenon on i-ID and the dithieno[3,2-*b*:2′,3′-*d*]silole copolymer exhibited a slight blue shift of about 5 nm from its absorption in solution to that in films.[26] Meanwhile, the broader ICT band in films than that in solution implies strong and more efficient charge transfer occurred in the solid state facilitating charge transport. The optical band gap ($E_{bg}^{optical}$), according to the equation $E_{bg}^{optical} = 1240/\lambda_{edge}$, was calculated to be 1.38 eV.

Molecular modelling

Density functional theory (DFT) was used to investigate the optimal geometric structure and the electronic configuration of **PDTPI**, this was done at the B3LYP/6-31G(d) level using Gaussian 09 and visualized with GaussView 5.0.9. To reduce the computational load, the aliphatic side-chains are reduced to methyl groups, as this has been shown in the literature not to affect the frontier orbital, while affecting the torsion angle to some extent.[26] As the system investigated was a polymer, two different methods of evaluation were set up. The first being simply one repetition of a donor unit and an acceptor unit, and the other was 3 consecutive donor acceptor units, thereby simulating a rather extended conjugation of polymers. Salvatori *et al.*[27] showed that this trimer setup gives decent results when simulating a similar system. The orbitals that are interesting in DFT modelling are the frontal orbitals *i.e.* the HOMO and LUMO. The geometrically optimized structures of both the single D–A and the three repeating D–A moieties are shown in Fig. 3. The dihedral angle between the single D–A model is

21.99°, and the 3 repeating D–A moieties all show similar angles ranging from 20.87 to −20.45° as seen in ESI Fig. S3.†

This continuous twist will afford a torsion on the backbone, thus explaining why there is practically no difference between the absorption of the film and the solution with less than 25 nm onset redshift.[28] The modelled torsion angle corresponds to the findings of Lei *et al.*[29] and Wang *et al.*[30] with angles similar to the modelling results, likewise this affords a small red shift onset of the solid state absorbance. While Wang *et al.* argue that the small change/redshift of the absorbance onset is ascribed to tight aggregation of the polymers in solution, this is seemingly also the case in **PDTPI** having this continuous torsion. Wang *et al.* also modeled a fluorinated i-ID moiety, which affords a very small torsion angle between the donor and the acceptor moiety (∼0.01°), following the argument the solvated polymeric interaction (π-stacking) should be significantly increased thus expecting a large red shift, which is not observed, indicating that even though the torsion angles are continuous, the angles are negligible and thus have a low effect on the π-stacking in both film and in solution. Although simplifications with regards to the side-chains were made, the true tendencies influencing the torsion angle are still valid.[27]

From the single D–A model, it is clear that the HOMO is primarily located on the donor moiety (DTP) and the LUMO is primarily located mainly on the (i-ID) moiety, as expected. This is also supported by the clear intermolecular charge transfer seen in the absorbance spectra, as described earlier.

The predicted HOMO and LUMO levels are −4.80 eV and −2.52 eV giving a band gap of 2.28 eV. This band gap differs from the experimentally determined levels, which is much lower (as the onset of absorbance is approximately 898 nm (Fig. 2)). The 3 repeating D–A units show the same tendencies with only a slight change in the predicted HOMO level given at −4.77 eV while the LUMO level is −2.69 eV. The computed band gap of the 3 repeating D–A units is 2.08 eV which still deviates from the experimental values. The modelling is in line with the findings of Zhuang *et al.*[31] who found that the frontier orbital of the LUMO and HOMO of a donor–acceptor polymer was primarily attributed to the acceptor and donor, respectively.

Frontier orbitals

To experimentally determine the frontier orbitals a CV experiment was performed as presented in ESI Fig. S2.† The oxidation onset was determined to be 0.98 V affording a HOMO level of −5.23 eV. The onset of the absorbance is determined to be 898 nm yielding an optical band gap of 1.38 eV. Using the optical band gap, the LUMO level is calculated to be −3.85 eV. Stalder *et al.*[32] reported that the placement of the LUMO should be in the range of −3.8 to −4 eV, which is supported by the CV findings. The found LUMO aligns well (as mentioned above) with the energy level −4.03 eV of PC[60]BM, although it is generally considered that 0.3 eV is the optimal LUMO$_{ACCEPTOR}$ − LUMO$_{DONOR}$ difference to ensure the highest charge separation. Even though the found difference of our system is slightly lower (0.2 eV), this is expected to be still sufficient to ensure charge separation. The LUMO of **PDTPI** is slightly higher than the LUMO
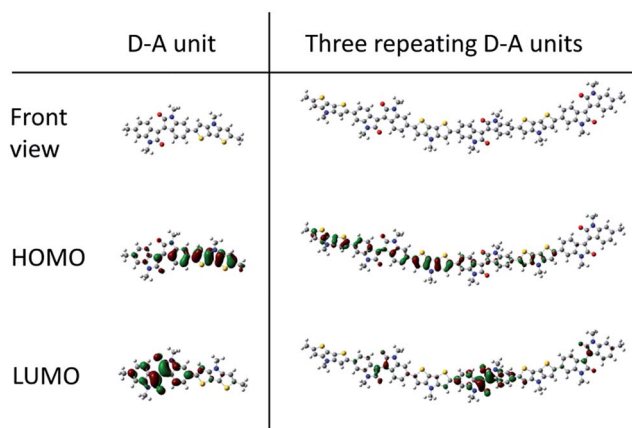

	D-A unit	Three repeating D-A units
Front view		
HOMO		
LUMO		

Fig. 3 DFT modelling at the B3LYP/6-31G(d) level by Gaussian 9 of the donor–acceptor model compound and for three consecutive D–A configurations.

1636 | *J. Mater. Chem. C*, 2015, **3**, 1633–1639

This journal is © The Royal Society of Chemistry 2015

reported by Wu *et al.*[17] where the LUMO of a similar polymer was determined to be −3.61 eV. The polymer reported by Wu *et al.* differs from **PDTPI** only in one extended thiophene on each side of the DTP moiety. Likewise the HOMO level of a similar polymer was found to be −4.94 eV, therefore the removal of thiophene will make **PDTPI** more stable under ambient conditions, while still maintaining the favorable LUMO level of i-ID. Comparing with the DFT simulations, the difference is rather large. This difference can be ascribed to two major contributions, first the fact that the relative conjugation length is rather low compared to the experimental data, which in reality is approximately 11 continuously linked D–A couples. Also the spatial dimension of the polymer is neglected in the DFT model applied, this means that the π–π stacking of the polymers is not evaluated. Despite the mismatch with the experimental values, the DFT model data are very similar to the previously reported DFT data at the B3LYP level, which are in the range of 2.8–3 eV.[27,31]

Photovoltaic properties

The photovoltaic properties of **PDTPI** were investigated by preparing flexible ITO-free organic solar cells in an inverted geometry with a bulk heterojunction active layer morphology consisting of **PDTPI** and PC[60]BM. Layer deposition was conducted both by spin coating and the more industrial scale suitable slot-die coating on a mini roll coater. The corresponding I–V curves and photovoltaic data, PCE, open circuit voltage (V_{OC}), short circuit current (J_{SC}), and fill factor (FF), can be seen in Fig. 4 and Table 1, respectively. The spin-coated devices exhibited a lower PCE (0.72%) than slot-die coated devices with the same composition. This is exclusively due to an increased J_{SC} for the slot-die coated devices. The improvement could be seen as an abnormality, since not only is the deposition method changed from spin-coating to slot-die coating, but also the area increases from 0.25 cm^2 to 1 cm^2, which would usually lead to a decreased J_{SC}. The observed increase can be explained by the utilization of a different PEDOT:PSS top-electrode where the spin-coated devices were based on Agfa EL-

Table 1 Performance data of the single junction roll-coated devices[a]

D : A	L (nm)	V_{OC} (V)	J_{SC} (mA cm^{-2})	FF (%)	PCE (%)
1 : 1	280	0.42 ± 0.01	−4.6 ± 0.2	32.3 ± 0.6	0.62 ± 0.05
1 : 2[b]	[c]	0.49	−3.69	40.3	0.72
1 : 2	180	0.45 ± 0.004	−4.95 ± 0.18	40.9 ± 1.1	0.92 ± 0.05
1 : 2	270	0.46 ± 0.004	−5.25 ± 0.28	41.3 ± 1.4	0.99 ± 0.08

[a] D: **PDTPI**, A: PC[60]BM, L: thickness. [b] Spin-coated sample. [c] Estimated active layer thickness was 160–200 nm.

P5010, the roll-coated devices had the 3 layer PEDOT:PSS electrode, as seen in Fig. 1. Meanwhile there must exist different morphologies caused by different solvent evaporation rates between the roll coating and spin coating process, this would have an impact, thus resulting in different short-circuit current density. However this is not the focus of this work, further studies on morphology effects, when going from spin coated to roll coated devices, could be pursued in the near future.

To optimize the **PDTPI** : PC[60]BM composition two different compositions (1 : 1 and 1 : 2) were tested. The results in Table 1 clearly reveal that the 1 : 2 composition is better, which besides an increase in PCE from 0.62% to 0.99% also showed improvement in the remaining photovoltaic characteristics.

The increase in FF by approximately 25% is the most significant, which may be explained by the improved interface or more likely improved carrier transport in the active layer, which together with a possible increase in exciton dissociation accounts for the increase in J_{SC} due to a reduced recombination. The film thickness was investigated by producing devices with 270 nm and 180 nm thick active layers. Reducing the film thickness resulted in a slight decrease in device efficiency due to a decrease in J_{SC} most likely due to a reduced absorption whereas the remaining photovoltaic characteristics were unaffected.

Better performing devices were therefore prepared with an active layer composition between **PDTPI** and PC[60]BM of 1 : 2 and a thickness of 280 nm, achieving a PCE of 0.99%, the J_{SC} of which was verified by EQE (seen in Fig. 5) which was found to be 5.30 mA cm^{-2} correlating nicely with the measured 5.25 mA cm^{-2} (see Table 1). These results however do not show the full potential of **PDTPI** since the Flextrode has a decreasing transmission from 60% to 35% in the interval of 600 nm to 900 nm (ref. 33) where **PDTPI** is photoactive (see Fig. 2).

The absorption characteristics of **PDTPI** which has a primary absorbance band in the 600–900 nm range (Fig. 2) could make it a prime candidate for the low band gap junction in tandem solar cells. **P3HT** and **PBDTTTz-4** were chosen as high band gap polymers due to their ideal spectral match with **PDTPI** as shown in Fig. 6.

Tandem solar cells were prepared using a roll coater by slot-die coating and flexographic printing *via* a method presented by Andersen *et al.*[22,34] the layer structure is shown in Fig. 1. The results from the three different tandem solar cell combinations prepared can be seen in Table 2. Fig. 7 shows the I–V characteristics of the 3 best performing devices with **PBDTTTz-4** and
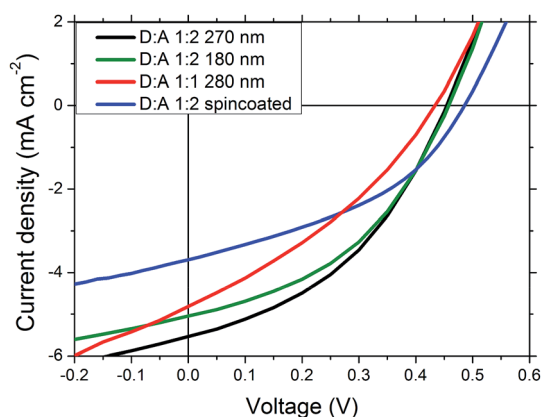

Fig. 4 I–V curves of roll coated and spin coated single junction solar cells with different **PDTPI**/PC[60]BM ratios and film thicknesses. The estimated thickness of the active layer in the spin coated cell (D : A 1 : 2) was 160–200 nm.
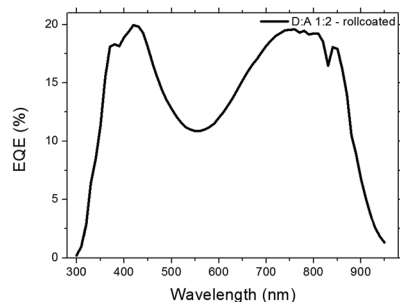
Fig. 5 EQE of the best performing single junction device, with a PDTPI/PC[60]BM ratio of 1 : 2 and an active layer thickness of 280 nm.
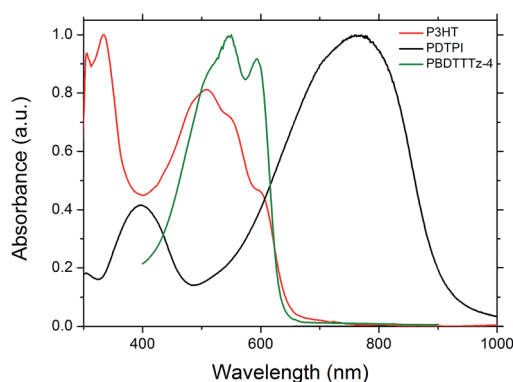

Fig. 6 The film absorbance of PBDTTTz-4 (green line), PDTPI (black line) and P3HT (red line).

P3HT combined with **PDTPI**. It is clear that the V_{OC} is lower than the theoretical maximum estimated from the sum of the single junction V_{OC}'s. This has however been reported previously in several cases when using flexible substrates[22,35,36] in which the tandem cell open-circuit voltages are 10–15% lower. Despite a close to ideal spectral overlap between **P3HT** and **PDPTI**, it is clear that the tandem solar cell consisting of **PDPTI** and **P3HT** underperforms, due to both lower J_{SC} and FF.

The efficiencies obtained for the **PBDTTTz-4** and **PDTPI** combination outperformed the **P3HT:PDTPI** combination with similar active layer thicknesses, mostly due to an increase in V_{OC}. The effects of layer thickness of tandem devices are clear when comparing the large difference in PCE for devices prepared with front junction thicknesses of 155 nm and 290 nm.

The increase in V_{OC} with increasing front junction thickness is likely due to the usage of the Flextrode which has been previously shown to contain rather large silver spikes;[22,35] as a
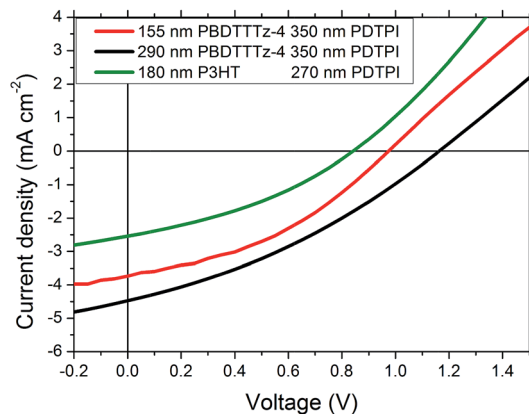

Fig. 7 $I–V$ characteristics of the tandem solar cells with the following combinations, 155 nm **PBDTTTz-4** 350 nm **PDTPI** (red line), 290 nm **PDBTTTz-4** 350 nm **PDTPI** (black line) and 180 nm **P3HT** 270 nm **PDTPI** (green line).

larger number of spikes will be embedded in the front junction relative to the back junction, increasing the front junction thickness will result in fewer penetrating silver spikes and hence the level of shunting will be reduced. The increase in J_{SC} can be ascribed to a better current matching between the junctions.

The best performing device showed a PCE of 1.73% and consists of a 290 nm **PBDTTTz-4** front junction and a 350 nm back junction of **PDTPI**, shown as the black line in Fig. 7.

Conclusions

A low-band gap polymer consisting of alternating di(2-ethylhexyl)isoindigo and *N*-(1-pentylhexyl)dithieno[3,2-*b*:2′,3′-*d*]-pyrrole moieties was synthesized. The synthesized polymer had a band gap of 1.38 eV with a HOMO level of −5.23 eV (determined by CV) and a suitably aligned LUMO level of −3.85 eV; which make it an ideal donor for the PC[60]BM. Density functional theory (DFT) computations showed that the LUMO was primarily located on the acceptor while the HOMO was primarily distributed on the donor moiety, i-ID and DTP, respectively. The DFT simulations also showed a torsion angle between the donor and acceptor moiety at around 22°, this combined with a simulation of an extended D–A structure showed a continuous torsion. This torsion could explain the relatively small onset redshift (∼25 nm) in absorbance when going from solution to film. Large area (0.25 to 1 cm²), ITO-free single junction photovoltaic devices showed efficiencies

Table 2 The layer composition and performance of the tandem solar cells, with **PDPTI** as a low band gap polymer, combined with **P3HT** or **PBDTTTz-4** as a high band gap polymer, respectively

Composition	V_{OC} (V)	J_{SC} (mA cm^{-2})	FF (%)	PCE (%)	Best PCE [%]
180 nm **P3HT** 270 nm **PDTPI**	0.85 ± 0.01	-2.49 ± 0.07	35.17 ± 0.05	0.74 ± 0.01	0.75
155 nm **PBDTTTz-4** 350 nm **PDTPI**	0.95 ± 0.02	2.83 ± 0.98	33.85 ± 3.84	1.12 ± 0.23	1.40
290 nm **PBDTTTz-4** 350 nm **PDTPI**	1.08 ± 0.09	4.60 ± 0.32	32.93 ± 0.52	1.63 ± 0.05	1.73

1638 | *J. Mater. Chem. C*, 2015, **3**, 1633–1639

This journal is © The Royal Society of Chemistry 2015

ranging from 0.72% to 0.99% for spin-coated and roll-coated devices, respectively. The low band gap and the EQE characteristics of **PDTPI** combined with the nice spectral overlap with **PBDTTTz-4** and **P3HT** made it an ideal candidate for a back cell in a tandem solar cell. Large area (0.8 cm^2), ITO-free roll-coated tandem junction photovoltaic devices were produced with efficiencies ranging 0.72% to 1.72%, for **PDTPI** combined with **P3HT** and **PBDTTTz-4**, respectively.

Acknowledgements

Notes and references

1 H. Xin, X. Guo, F. S. Kim, G. Ren, M. D. Watson and S. A. Jenekhe, *J. Mater. Chem.*, 2009, **19**, 5303–5310.

2 X. Guo, F. S. Kim, M. J. Seger, S. A. Jenekhe and M. D. Watson, *Chem. Mater.*, 2012, **24**, 1434–1442.

3 X. Zhan, Z. Tan, E. Zhou, Y. Li, R. Misra, A. Grant, B. Domercq, X.-H. Zhang, Z. An, X. Zhang, S. Barlow, B. Kippelen and S. R. Marder, *J. Mater. Chem.*, 2009, **19**, 5794–5803.

4 B. A. D. Neto, A. A. M. Lapis, E. N. da Silva Jr and J. Dupont, *Eur. J. Org. Chem.*, 2013, 228–255.

5 S. Qu and H. Tian, *Chem. Commun.*, 2012, **48**, 3039–3051.

6 W. Yue, X. Huang, J. Yuan, W. Ma, F. C. Krebs and D. Yu, *J. Mater. Chem. A*, 2013, **1**, 10116–101119.

7 B. R. Aïch, S. Beaupré, M. Leclerc and Y. Tao, *Org. Electron.*, 2014, **15**, 543–548.

8 R. Stalder, J. Mei and J. R. Reynolds, *Macromolecules*, 2010, **43**, 8348–8352.

9 E. Bundgaard and F. Krebs, *Sol. Energy Mater. Sol. Cells*, 2007, **91**, 954–985.

10 J.-L. Brédas, D. Beljonne, V. Coropceanu and J. Cornil, *Chem. Rev.*, 2004, **104**, 4971–5004.

11 J. Mei, K. R. Graham, R. Stalder and J. R. Reynolds, *Org. Lett.*, 2010, **12**, 660–663.

12 G. Zhang, Y. Fu, Z. Xie and Q. Zhang, *Macromolecules*, 2011, **44**, 1414–1420.

13 B. Liu, Y. Zou, B. Peng, B. Zhao, K. Huang, Y. He and C. Pan, *Polym. Chem.*, 2011, **2**, 1156–1162.

14 E. Wang, Z. Ma, Z. Zhang, P. Henriksson, O. Inganäs, F. Zhang and M. R. Andersson, *Chem. Commun.*, 2011, **47**, 4908–4910.

15 E. Wang, Z. Ma, Z. Zhang, K. Vandewal, P. Henriksson, O. Inganäs, F. Zhang and M. R. Andersson, *J. Am. Chem. Soc.*, 2011, **133**, 14244–14247.

16 Y. Deng, J. Liu, J. Wang, L. Liu, W. Li, H. Tian, X. Zhang, Z. Xie, Y. Geng and F. Wang, *Adv. Mater.*, 2014, **26**, 471–476.

17 F. Wu, H. Yang, C. M. Li and J. Qin, *Polym. Adv. Technol.*, 2013, **24**, 945–950.

18 F. C. Krebs, *Sol. Energy Mater. Sol. Cells*, 2009, **93**, 1636–1641.

19 F. C. Krebs, *Org. Electron.*, 2009, **10**, 761–768.

20 W. Yue, T. T. Larsen-Olsen, X. Hu, M. Shi, H. Chen, M. Hinge, P. Fojan, F. C. Krebs and D. Yu, *J. Mater. Chem. A*, 2013, **1**, 1785–1793.

21 D. Angmo, S. A. Gevorgyan, T. T. Larsen-Olsen, R. R. Søndergaard, M. Hösel, M. Jørgensen, R. Gupta, G. U. Kulkarni and F. C. Krebs, *Org. Electron.*, 2013, **14**, 984–994.

22 T. R. Andersen, H. F. Dam, B. Andreasen, M. Hösel, M. V. Madsen, S. A. Gevorgyan, R. R. Søndergaard, M. Jørgensen and F. C. Krebs, *Sol. Energy Mater. Sol. Cells*, 2014, **120**, 735–743.

23 M. M. Wienk, M. Turbiez, J. Gilot and R. A. J. Janssen, *Adv. Mater.*, 2008, **20**, 2556–2560.

24 R. C. Coffin, J. Peet, J. Rogers and G. C. Bazan, *Nat. Chem.*, 2009, **1**, 657–661.

25 C.-C. Ho, S.-Y. Chang, T.-C. Huang, C.-A. Chen, H.-C. Liao, Y.-F. Chen and W.-F. Su, *Polym. Chem.*, 2013, **4**, 5351–5360.

26 R. Stalder, C. Grand, J. Subbiah, F. So and J. R. Reynolds, *Polym. Chem.*, 2012, **3**, 89–92.

27 P. Salvatori, E. Mosconi, E. Wang, M. Andersson, M. Muccini and F. De Angelis, *J. Phys. Chem. C*, 2013, **117**, 17940–17954.

28 S. Zhang, H. Fan, Y. Liu, G. Zhao, Q. Li, Y. Li and X. Zhan, *J. Polym. Sci., Part A: Polym. Chem.*, 2009, **47**, 2843–2852.

29 T. Lei, J.-H. Dou, Z.-J. Ma, C.-H. Yao, C.-J. Liu, J.-Y. Wang and J. Pei, *J. Am. Chem. Soc.*, 2012, **134**, 20025–20028.

30 Z. Wang, J. Zhao, Y. Li and Q. Peng, *Polym. Chem.*, 2014, **5**, 4984–4992.

31 W. Zhuang, M. Bolognesi, M. Seri, P. Henriksson, D. Gedefaw, R. Kroon, M. Jarvid, A. Lundin, E. Wang, M. Muccini and M. R. Andersson, *Macromolecules*, 2013, **46**, 8488–8499.

32 R. Stalder, J. Mei, K. R. Graham, L. A. Estrada and J. R. Reynolds, *Chem. Mater.*, 2014, **26**, 664–678.

33 M. Hösel, R. R. Søndergaard, M. Jørgensen and F. C. Krebs, *Energy Technol.*, 2013, **1**, 102–107.

34 T. R. Andersen, H. F. Dam, M. Hösel, M. Helgesen, J. E. Carlé, T. T. Larsen-Olsen, S. a. Gevorgyan, J. W. Andreasen, J. Adams, N. Li, F. Machui, G. D. Spyropoulos, T. Ameri, N. Lemaître, M. Legros, A. Scheel, D. Gaiser, K. Kreul, S. Berny, O. R. Lozman, S. Nordman, M. Välimäki, M. Vilkman, R. R. Søndergaard, M. Jørgensen, C. J. Brabec and F. C. Krebs, *Energy Environ. Sci.*, 2014, **7**, 2925–2933.

35 T. R. Andersen, H. F. Dam, B. Burkhart, D. Angmo, M. Corazza, B. C. Thompson and F. C. Krebs, *J. Mater. Chem. C*, 2014, **2**, 9412–9415.

36 N. Li, D. Baran, G. D. Spyropoulos, H. Zhang, S. Berny, M. Turbiez, T. Ameri, F. C. Krebs and C. J. Brabec, *Adv. Energy Mater.*, 2014, **4**, 1400084.

37 M. Zhang, Y. Sun, X. Guo, C. Cui, Y. He and Y. Li, *Macromolecules*, 2011, **44**, 7625–7631.

38 M. Helgesen, J. E. Carle and F. C. Krebs, *Adv. Energy Mater.*, 2013, **3**, 1664–1669.

This journal is © The Royal Society of Chemistry 2015

J. Mater. Chem. C, 2015, **3**, 1633–1639 | 1639